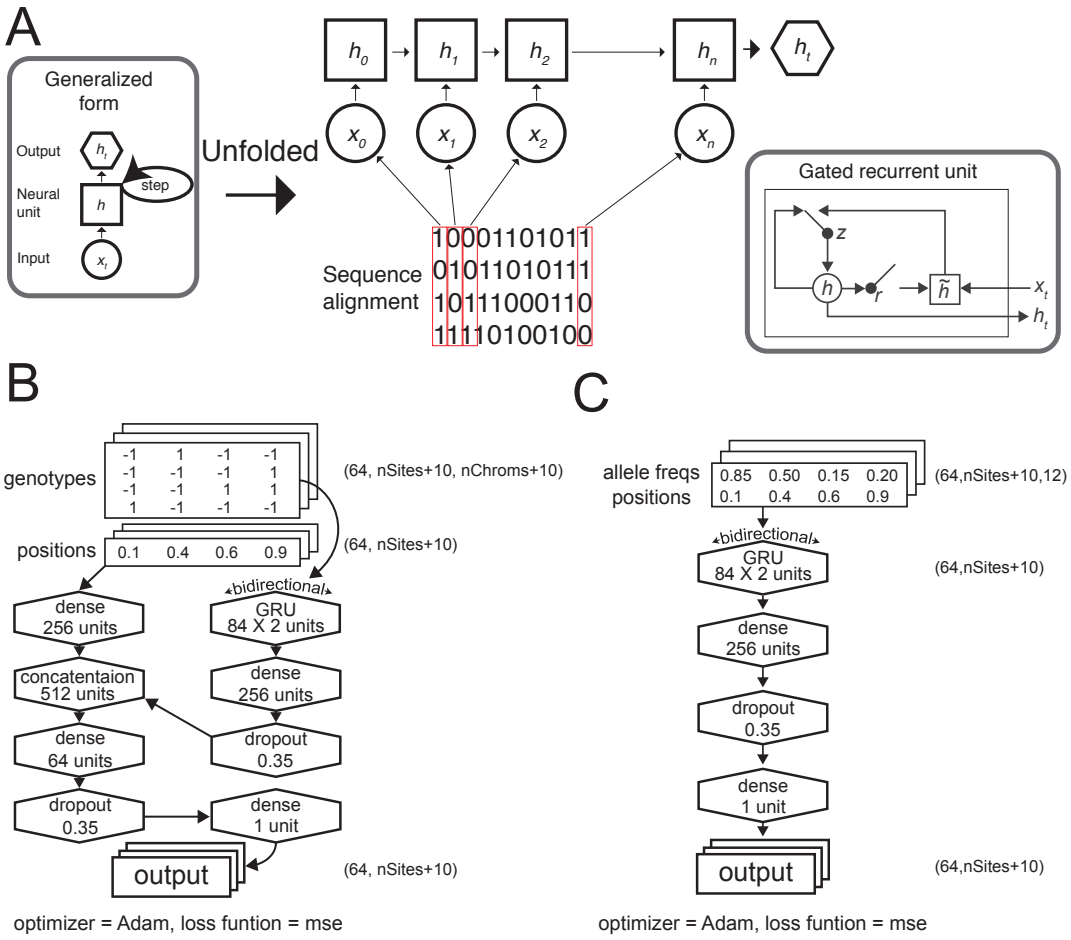


**Figure S1** **(A, left)** Generalized form for a recurrent neural network trained on a genomic sequence alignment. **(A, right)** Generalized form of each gated recurrent unit, where $r$, $z$, $h_t$, and $\tilde{h}_t$ correspond to the reset gate, update gate, activation, and candidate activation, respectively (***Cho et al., 2014***). **(B)** Cartoon depicting the neural network architectures used in ReLERNN for individually sequenced genomes or **(C)** pooled sequences. Tensor shapes are shown for the default parameters [$batchsize = 64$, $padsize = 5$].

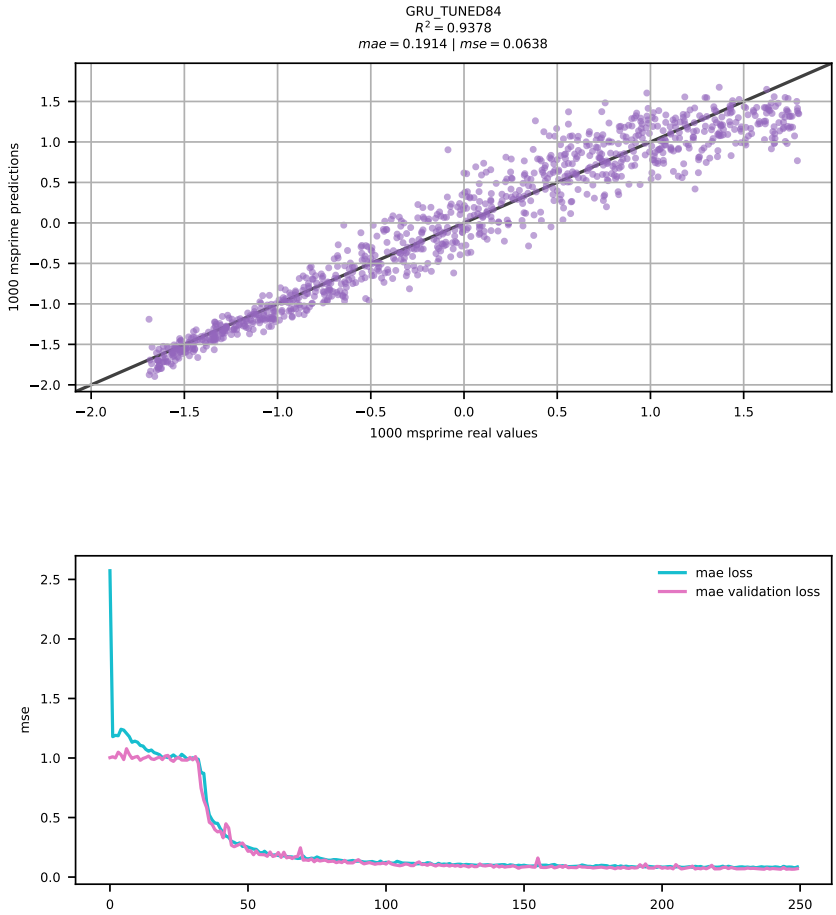


**Figure S2** ReLERNN training and test results. **(Top)** Scatter plot of raw (unnormalized) predictions for 1000 test examples using ReLERNN with the same parameters used in ***Figure 2***. Mean absolute error and mean squared error are shown. **(Bottom)** Line graph showing the convergence of loss (measured by mean squared error) over time (epochs) during training on the same data as above, for both the training set (blue lines) and the validation set (purple lines).

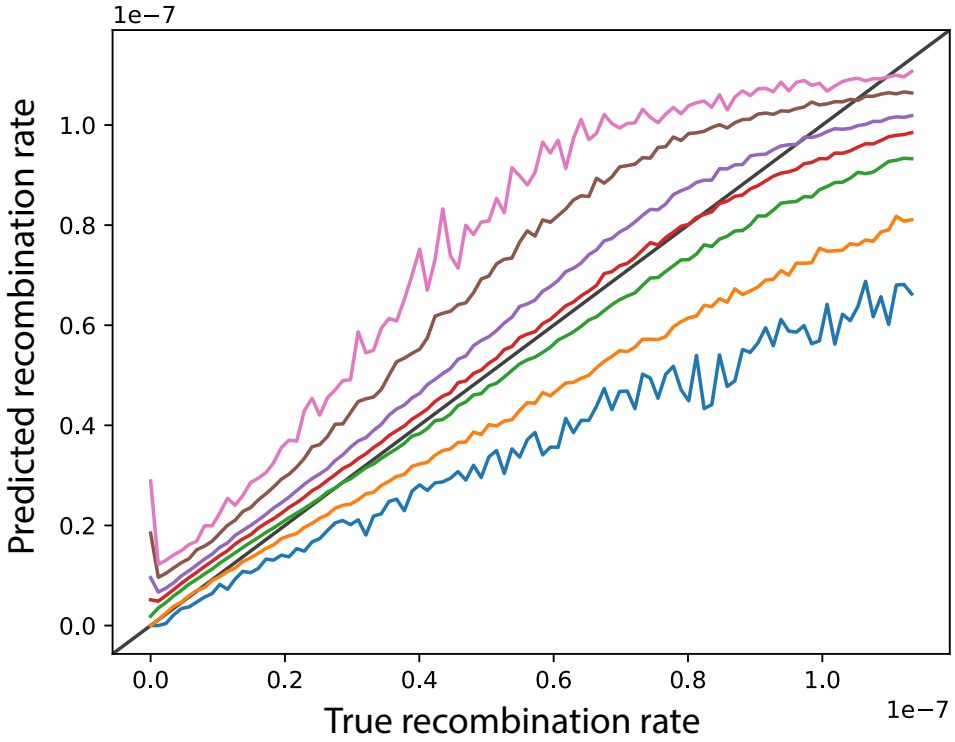


**Figure S3** A characteristic example distribution of parametric bootstraping predictions, as implemented by `ReLERNN_BSCORRECT`. Lines represent the minimum (blue), lower 5% (orange), lower 25% (green), median (red), upper 25% (purple), upper 95% (brown), and maximum (pink) bounds for each of 1000 replicate simulations and predictions (y-axis) across 100 recombination rate bins (x-axis)

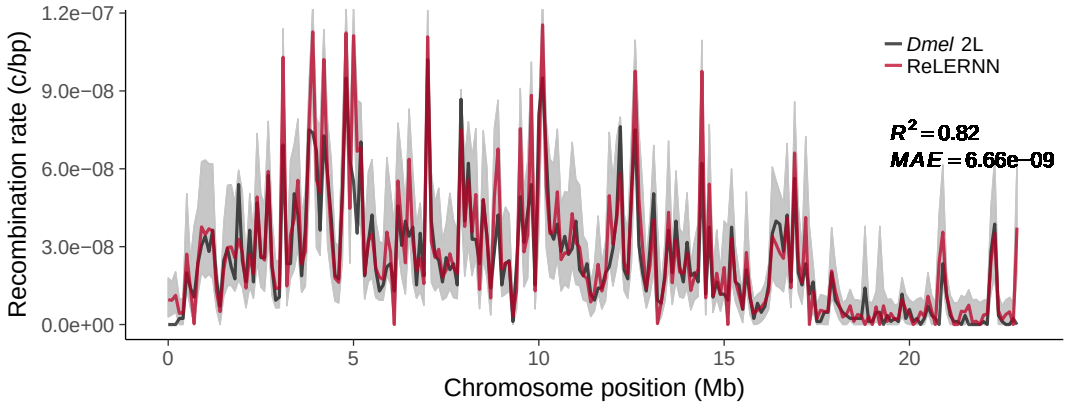


**Figure S4** Recombination rate predictions for a simulated *Drosophila* chromosome (black line) using ReLERNN (red line). The recombination landscape was simulated for $n = 4$ chromosomes under mutation-drift equilibrium using msprime (***Kelleher et al., 2016***), with per-base crossover rates derived from *D. melanogaster* chromosome 2L (***Comeron et al., 2012***). Gray ribbons represent 95% confidence intervals. $R^2$ is reported for the general linear model of predicted rates on true rates and mean absolute error was calculated across all 100 kb windows.

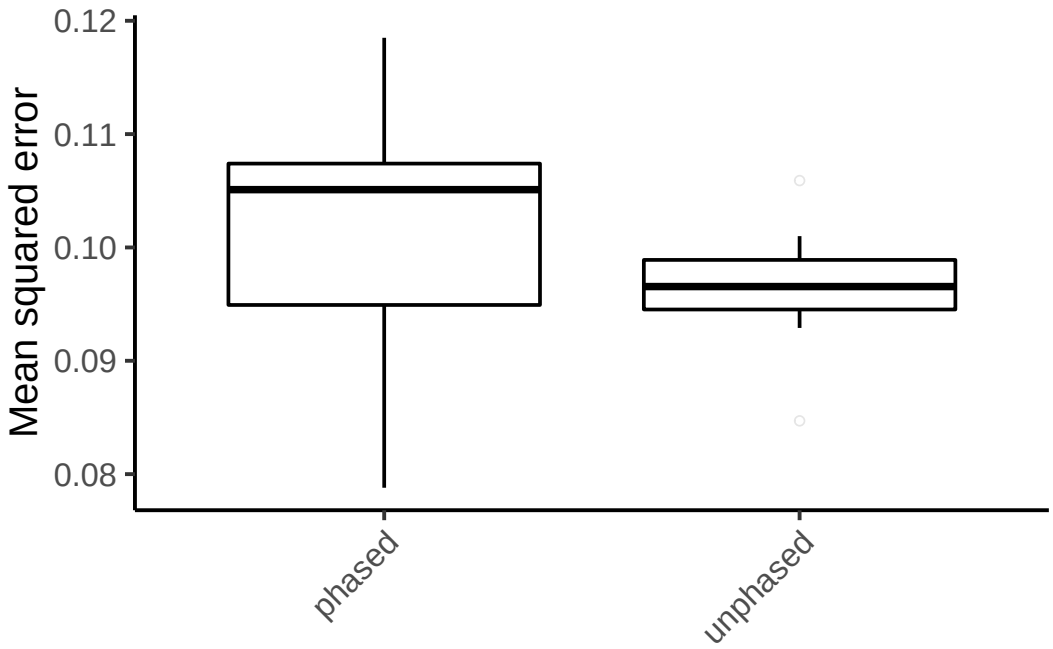


**Figure S5** Mean squared error for ReLERNN predictions on 10 replicates of 1000 test simulations using 100% correctly phased input genotypes and completely unphased genotypes. All simulations used the recombination map derived from *D. melanogaster* chromosome 2L (***Comeron et al., 2012***).

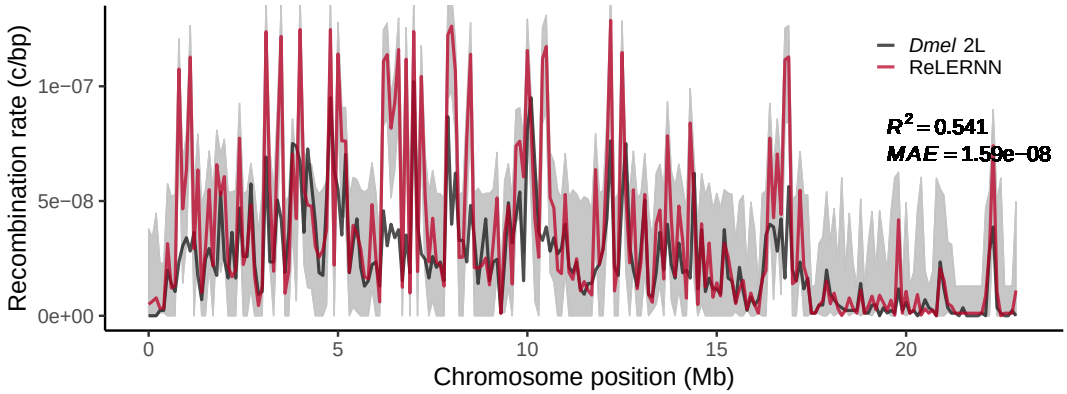


**Figure S6** Recombination rate predictions from Pool-seq data for a simulated *Drosophila* chromosome (black line) using ReLERNN (red line). The recombination landscape was simulated for $n = 50$ chromosomes and a read depth of $50X$, under mutation-drift equilibrium using msprime (***Kelleher et al., 2016***), with per-base crossover rates derived from *D. melanogaster* chromosome 2L (***Comeron et al., 2012***). Gray ribbons represent 95% confidence intervals. $R^2$ is reported for the general linear model of predicted rates on true rates and mean absolute error was calculated across all 100 kb windows.

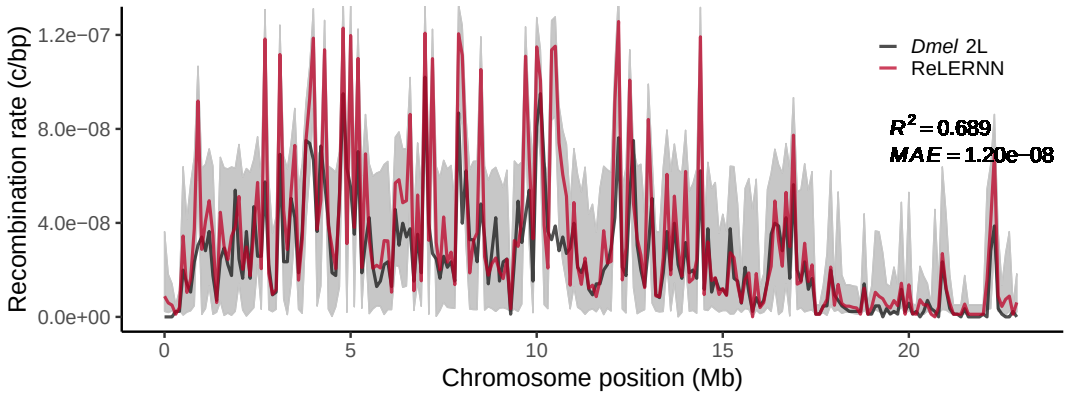


**Figure S7** Recombination rate predictions from Pool-seq data for a simulated *Drosophila* chromosome (black line) using ReLERNN (red line). The recombination landscape was simulated for $n = 50$ chromosomes and a read depth of $250X$, under mutation-drift equilibrium using msprime (***Kelleher et al., 2016***), with per-base crossover rates derived from *D. melanogaster* chromosome 2L (***Comeron et al., 2012***). Gray ribbons represent 95% confidence intervals. $R^2$ is reported for the general linear model of predicted rates on true rates and mean absolute error was calculated across all 100 kb windows.

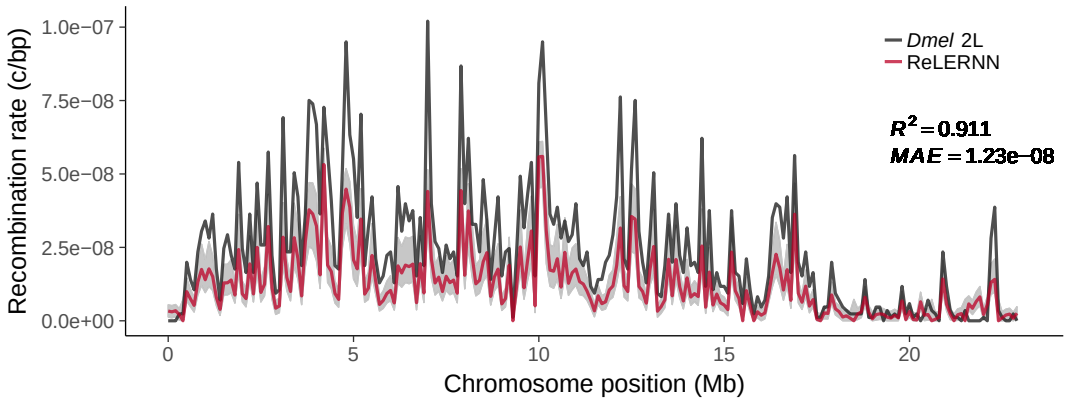


**Figure S8** Recombination rate predictions for a simulated *Drosophila* chromosome (black line) using ReLERNN (red line). The recombination landscape was simulated for $n = 20$ chromosomes under mutation-drift equilibrium using msprime (***Kelleher et al., 2016***), with per-base crossover rates derived from *D. melanogaster* chromosome 2L (***Comeron et al., 2012***). Here the per-base mutation rate was assumed to be 50% less than the rate used for simulation. Gray ribbons represent 95% confidence intervals. $R^2$ is reported for the general linear model of predicted rates on true rates and mean absolute error was calculated across all 100 kb windows.

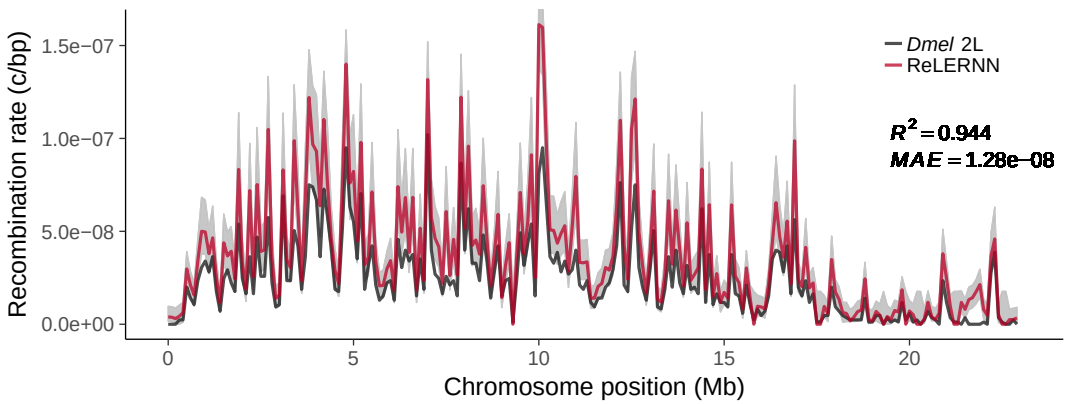


**Figure S9** Recombination rate predictions for a simulated *Drosophila* chromosome (black line) using ReLERNN (red line). The recombination landscape was simulated for $n = 20$ chromosomes under mutation-drift equilibrium using msprime (***Kelleher et al., 2016***), with per-base crossover rates derived from *D. melanogaster* chromosome 2L (***Comeron et al., 2012***). Here the per-base mutation rate was assumed to be 50% greater than the rate used for simulation. Gray ribbons represent 95% confidence intervals. $R^2$ is reported for the general linear model of predicted rates on true rates and mean absolute error was calculated across all 100 kb windows.

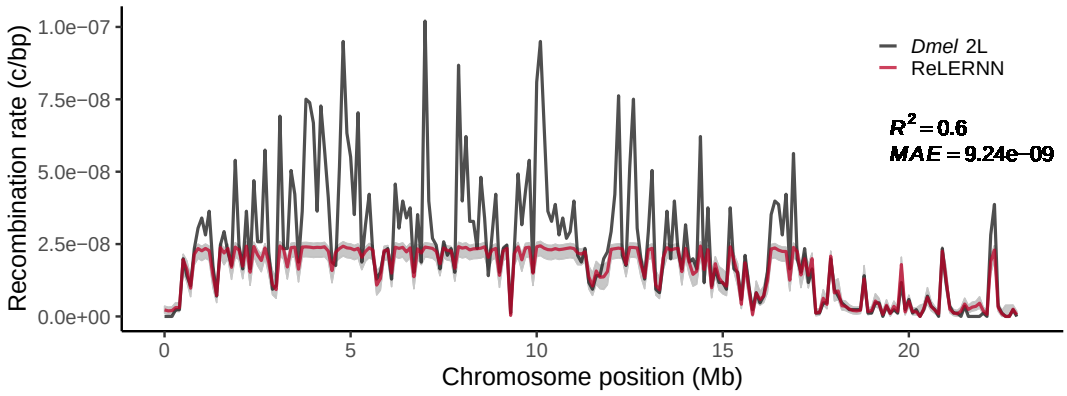


**Figure S10** Recombination rate predictions for a simulated *Drosophila* chromosome (black line) using ReLERNN (red line). The recombination landscape was simulated for $n = 20$ chromosomes under mutation-drift equilibrium using msprime (***Kelleher et al., 2016***), with per-base crossover rates derived from *D. melanogaster* chromosome 2L (***Comeron et al., 2012***). Here the per-base mutation rate was assumed to be equal to the true rate, but $\rho_{max}$ was assumed to be $\frac{\rho_{max}}{5}$. Gray ribbons represent 95% confidence intervals. $R^2$ is reported for the general linear model of predicted rates on true rates and mean absolute error was calculated across all 100 kb windows.

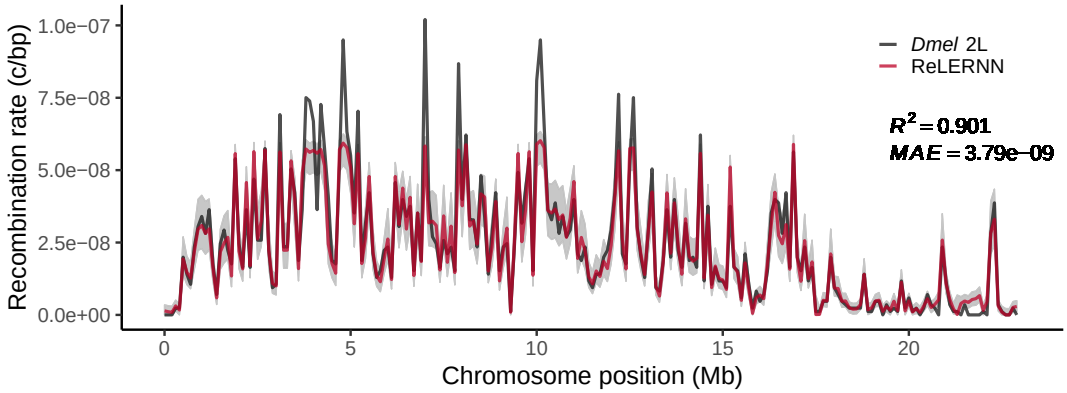


**Figure S11** Recombination rate predictions for a simulated *Drosophila* chromosome (black line) using ReLERNN (red line). The recombination landscape was simulated for $n = 20$ chromosomes under mutation-drift equilibrium using msprime (***Kelleher et al., 2016***), with per-base crossover rates derived from *D. melanogaster* chromosome 2L (***Comeron et al., 2012***). Here the per-base mutation rate was assumed to be equal to the true rate, but $\rho_{max}$ was assumed to be $\frac{\rho_{max}}{2}$. Gray ribbons represent 95% confidence intervals. $R^2$ is reported for the general linear model of predicted rates on true rates and mean absolute error was calculated across all 100 kb windows.

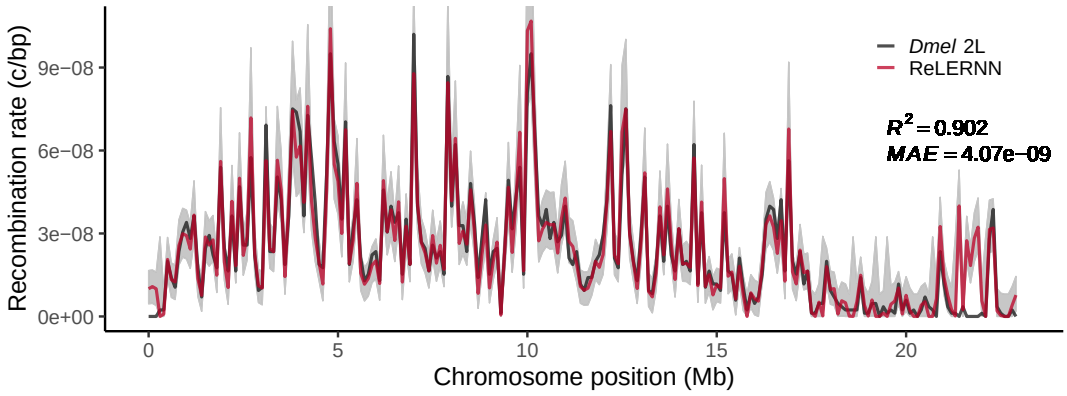


**Figure S12** Recombination rate predictions for a simulated *Drosophila* chromosome (black line) using ReLERNN (red line). The recombination landscape was simulated for $n = 20$ chromosomes under mutation-drift equilibrium using msprime (***Kelleher et al., 2016***), with per-base crossover rates derived from *D. melanogaster* chromosome 2L (***Comeron et al., 2012***). Here the per-base mutation rate was assumed to be equal to the true rate, but $\rho_{max}$ was assumed to be $2\rho_{max}$. Gray ribbons represent 95% confidence intervals. $R^2$ is reported for the general linear model of predicted rates on true rates and mean absolute error was calculated across all 100 kb windows.

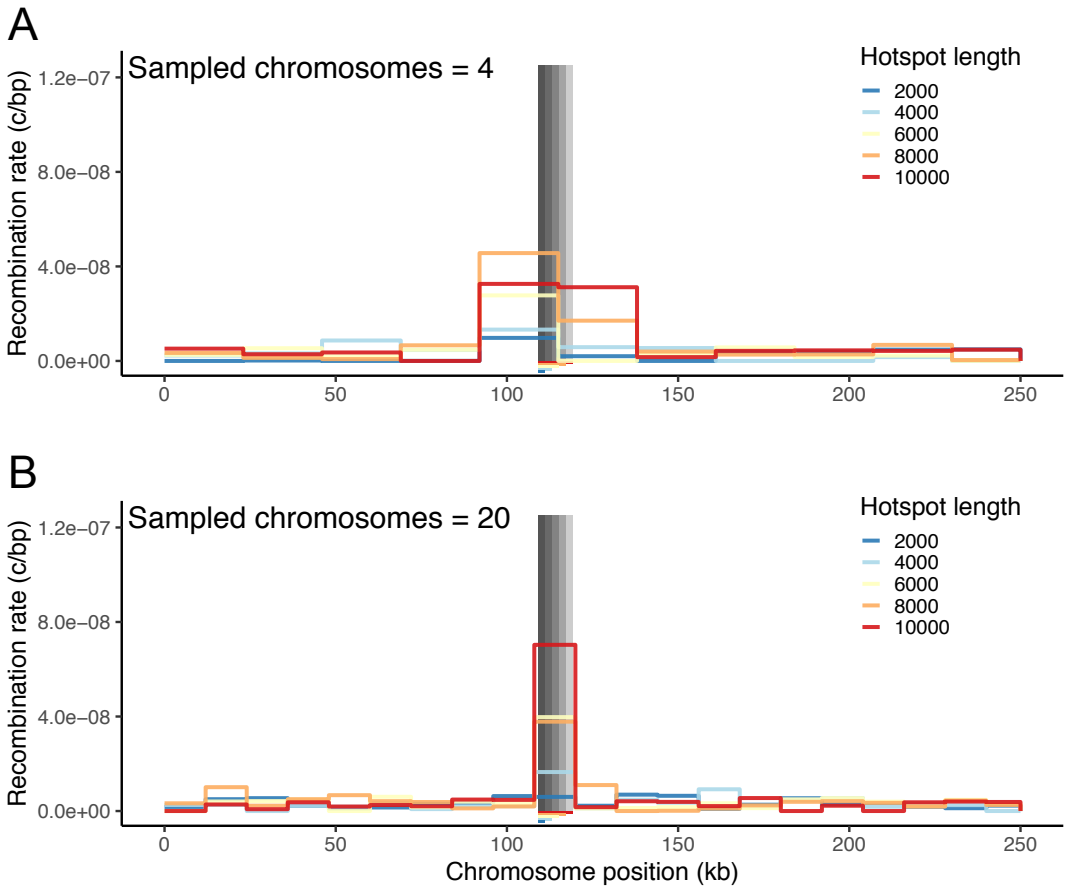


**Figure S13 (A)** Fine-scale rate predictions generated by ReLERNN for simulated recombination hotspots of varying lengths ($length \in \{2kb, 4kb, 6kb, 8kb, 10kb\}$, $r_{background} = 2.5e^{-9}$, $r_{hotspot} = 1.25e^{-7}$) for $n = 4$ and **(B)** $n = 20$ chromosomes.

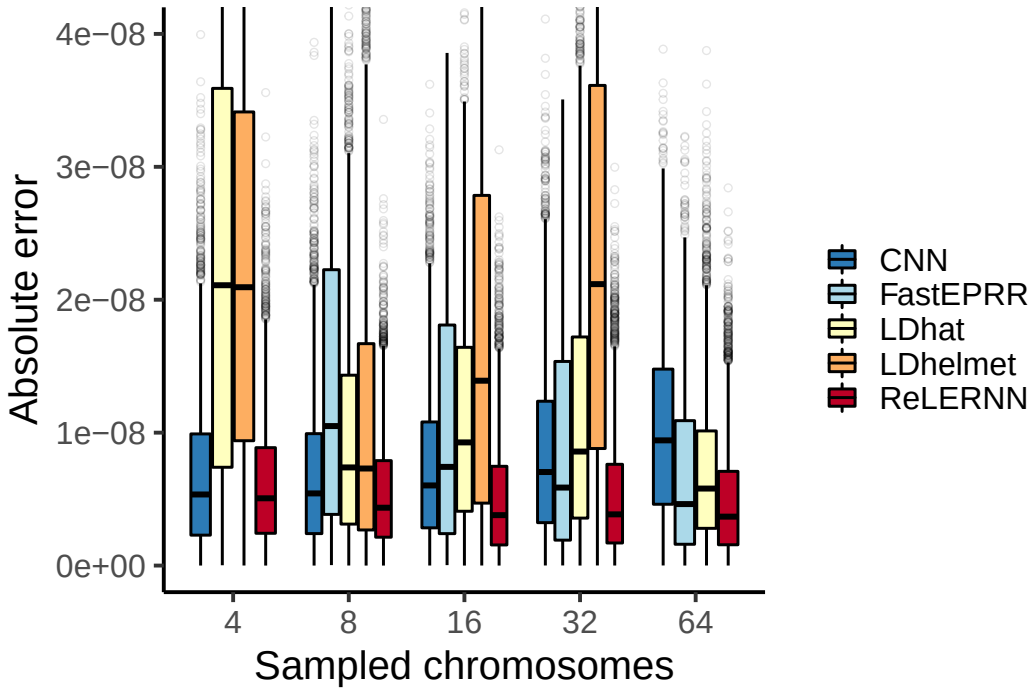


**Figure S14** Distribution of absolute error ($|r_{predicted} - r_{true}|$) for each method across 5000 simulated chromosomes (1000 for FastEPRR). Independent simulations were run under a model of demographic equilibrium. Sampled chromosomes indicate the number of independent sequences that were sampled from each msprime (***Kelleher et al., 2016***) coalescent simulation. LDhelmet was not able be used with $n = 64$ chromosomes, and FastEPRR was not able to be used with $n = 4$.

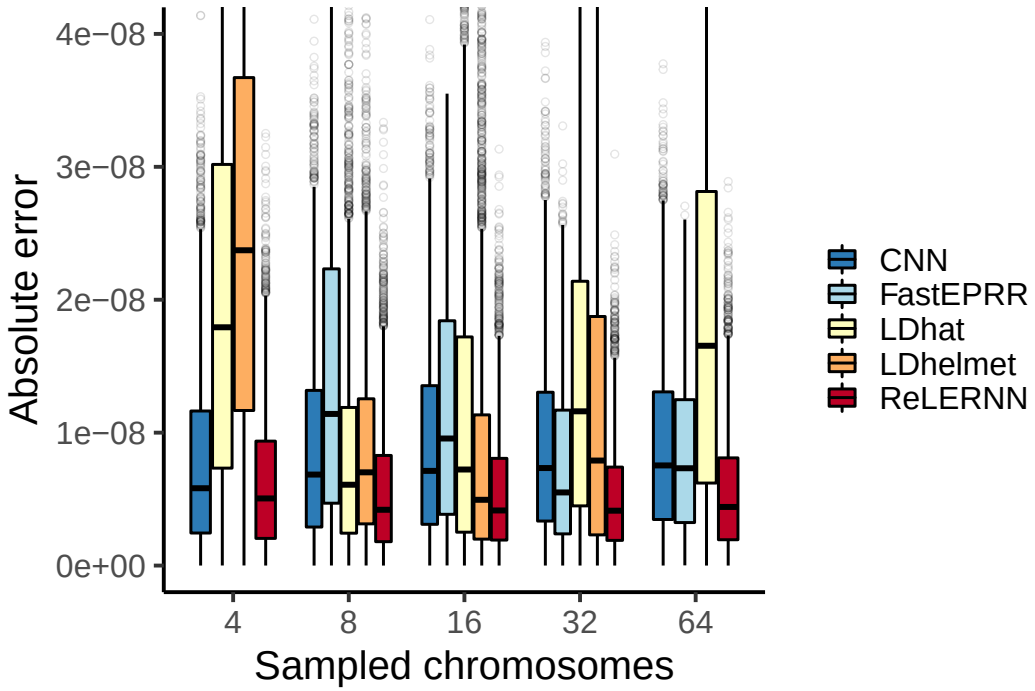


**Figure S15** Distribution of absolute error ($|r_{predicted} - r_{true}|$) for each method across 5000 simulated chromosomes (1000 for FastEPRR). Independent simulations were run under a model of population size expansion (see methods). Sampled chromosomes indicate the number of independent sequences that were sampled from each msprime (***Kelleher et al., 2016***) coalescent simulation. LDhelmet was not able be used with $n = 64$ chromosomes, and FastEPRR was not able to be used with $n = 4$.

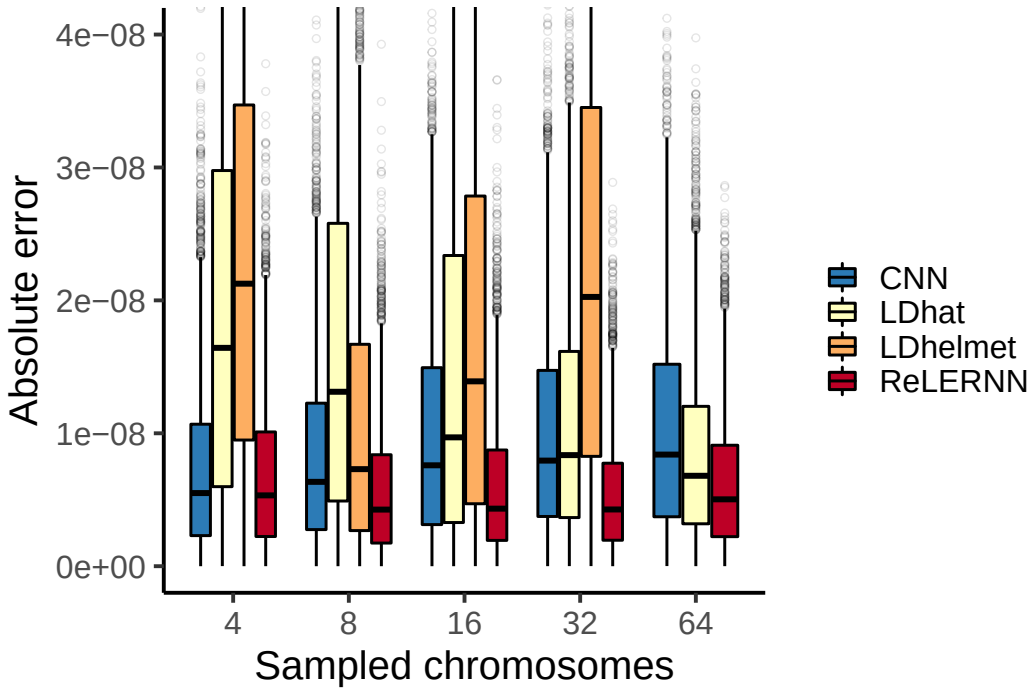


**Figure S16** Distribution of absolute error ($|r_{predicted} - r_{true}|$) for each method across 5000 simulated chromosomes after model misspecification. For the CNN and ReLERNN, predictions were made by training on demographic simulations while testing on sequences simulated under equilibrium. For LDhat and LDhelmet, the lookup tables were generated using parameters values that were estimated from simulations where the model was misspecified in the same way as described for the CNN and ReLERNN above. Sampled chromosomes indicate the number of independent sequences that were sampled from each msprime (***Kelleher et al., 2016***) coalescent simulation. LDhelmet was not able be used with $n = 64$ chromosomes and the demographic model could not be intentionally misspecified using FastEPRR.

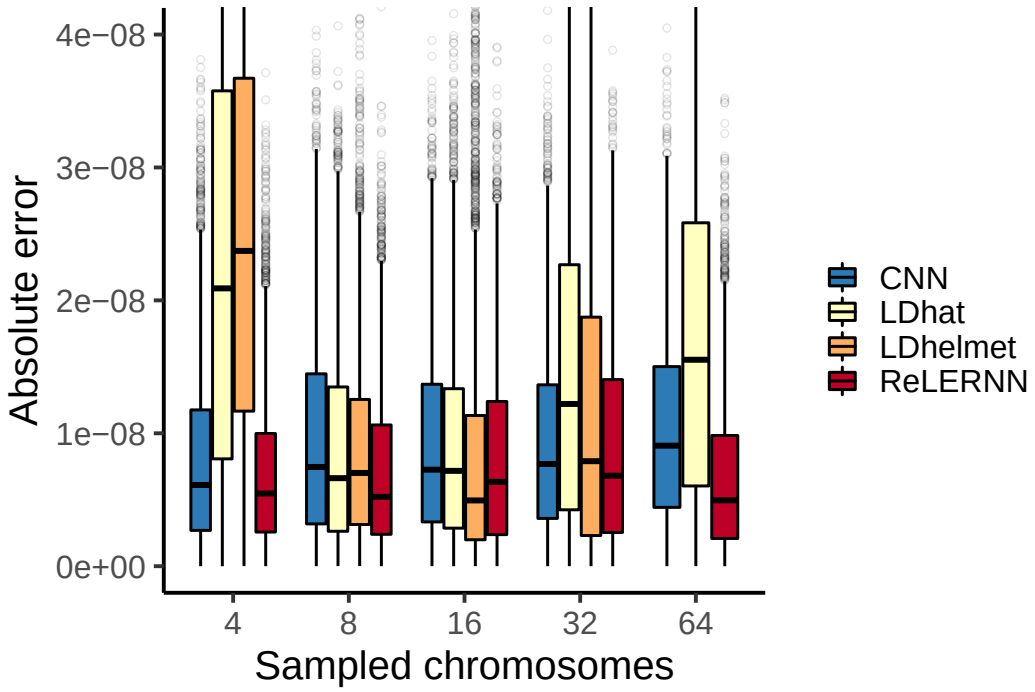


**Figure S17** Distribution of absolute error ($|r_{predicted} - r_{true}|$) for each method across 5000 simulated chromosomes after model misspecification. For the CNN and ReLERNN, predictions were made by training on equilibrium simulations while testing on sequences simulated under a model of population size expansion. For LDhat and LDhelmet, the lookup tables were generated using parameters values that were estimated from simulations where the model was misspecified in the same way as described for the CNN and ReLERNN above. Sampled chromosomes indicate the number of independent sequences that were sampled from each msprime (***Kelleher et al., 2016***) coalescent simulation. LDhelmet was not able be used with $n = 64$ chromosomes and the demographic model could not be intentionally misspecified using FastEPRR.

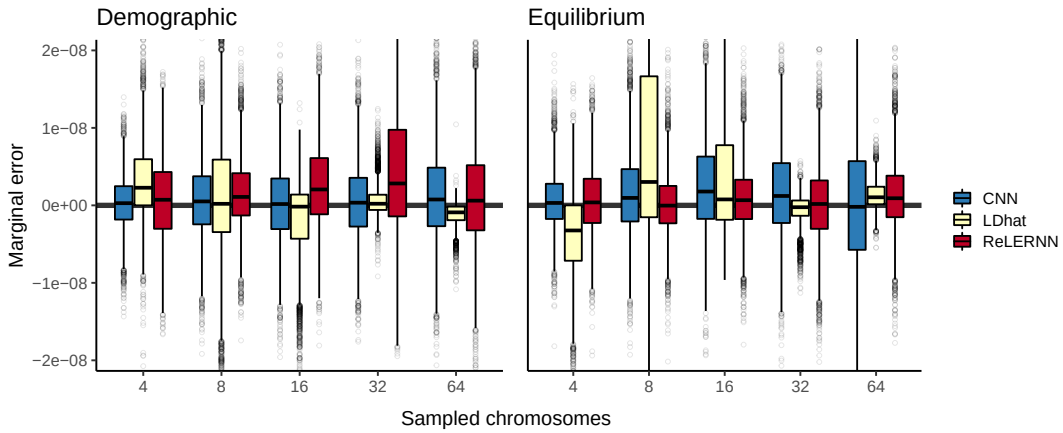


**Figure S18** Distribution of marginal error attributed to model misspecification across 5000 simulated chromosomes. Predictions were made by training on equilibrium simulations and testing on sequences simulated under a demographic model **(left)** or training on demographic simulations and testing on sequences simulated under equilibrium **(right)**. Here, marginal error is represented as $\epsilon_m - \epsilon_c$, where $\epsilon_m$ and $\epsilon_c$ are equal to $|r_{predicted} - r_{true}|$ when the model is misspecified and correctly specified, respectively. Sampled chromosomes indicate the number of independent sequences that were sampled from each msprime (***Kelleher et al., 2016***) coalescent simulation.

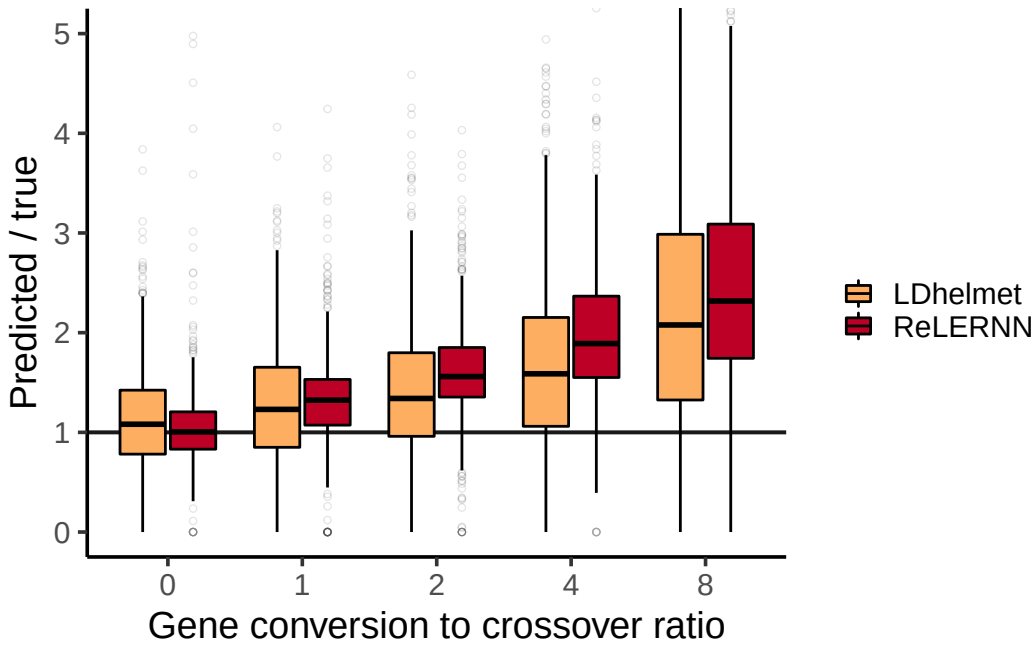


**Figure S19** Distribution of predicted rates of recombination over true rates for 5000 examples simulated with gene conversion and $n = 8$. The ratio of gene conversion to crossovers was drawn from $U(0, \frac{r_{GC}}{r_{CO}})$, with $\frac{r_{GC}}{r_{CO}} \in \{0, 1, 2, 4, 8\}$. Gene conversion tract lengths were fixed at 352 bp. All simulations were completed in ms (***Hudson, 2002***).

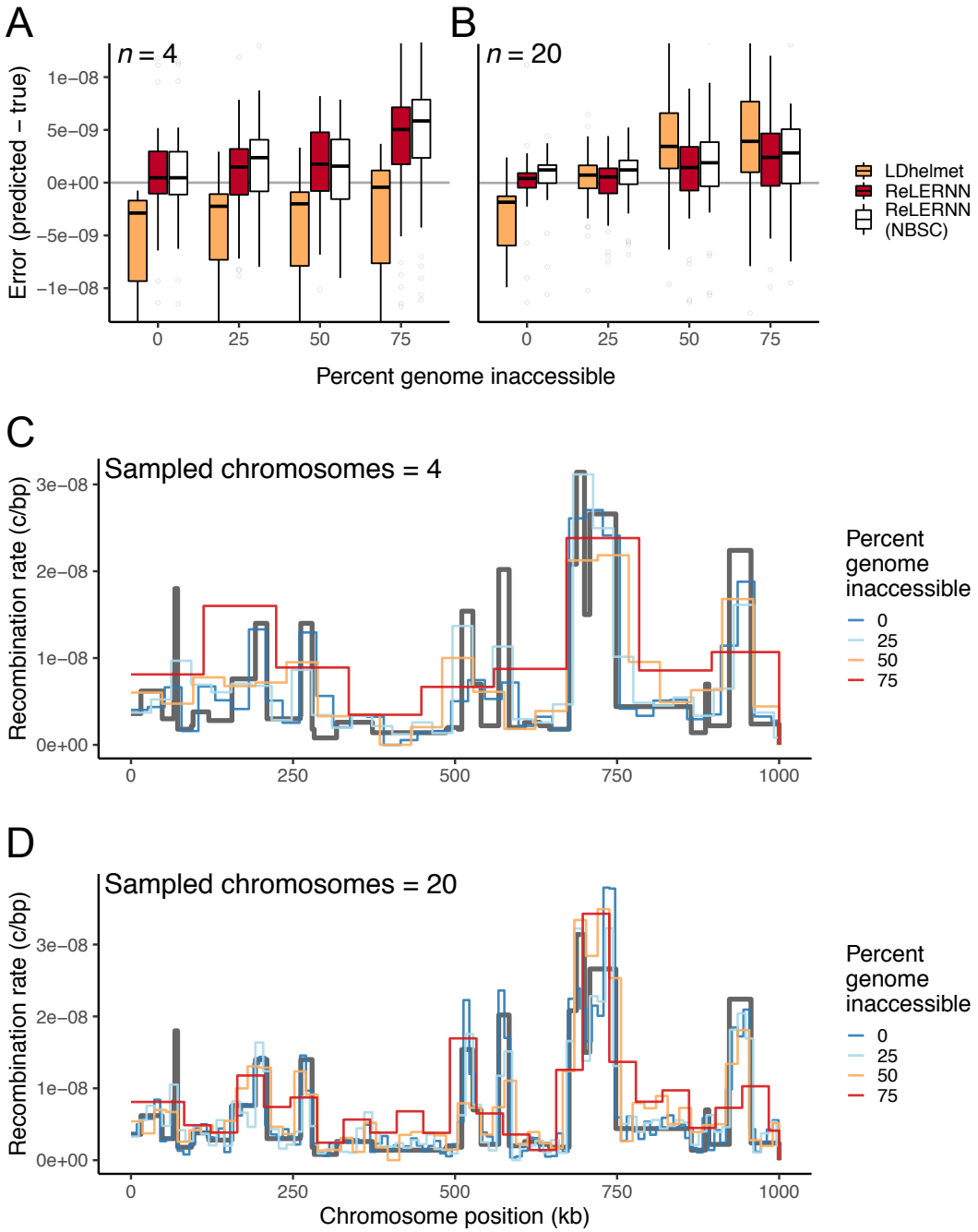


**Figure S20 (A)** Distribution of raw error ($r_{predicted} - r_{true}$) for LDhelmet (***Chan et al., 2012***) and ReLERNN when presented with varying levels of genome inaccessibility for simulations with $n = 4$ and **(B)** $n = 20$ chromosomes. **(C)** Fine-scale rate predictions generated by ReLERNN for a recombination landscape (grey line) simulated with varying levels of genome inaccessibility, for $n = 4$ and **(D)** $n = 20$ chromosomes.

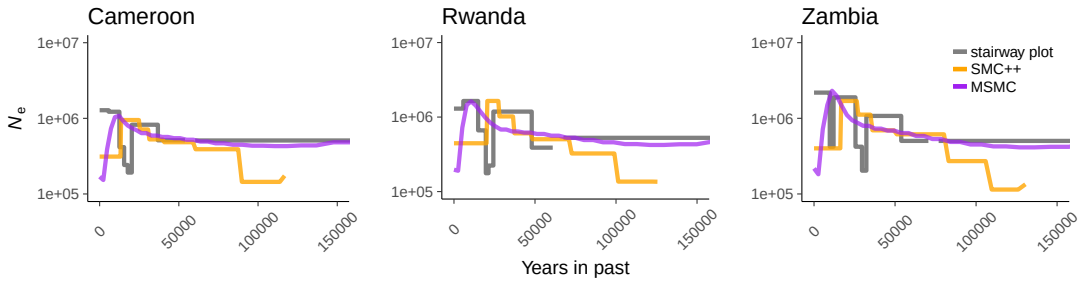


**Figure S21** Historical population size estimates were inferred for Cameroon, Rwanda, and Zambia using three separate methods, all of which disagree with one another. Inferences are based on 10 samples for both stairwayplot (grey line) and SMC++ (orange line), and 2 samples for MSMC (purple line).

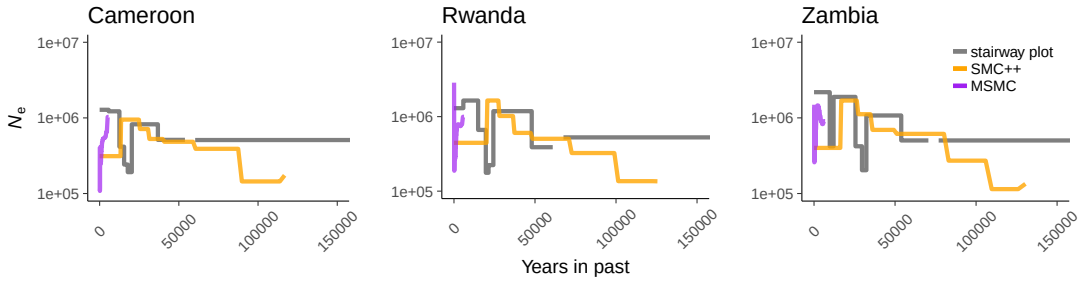


**Figure S22** Historical population size estimates were inferred for Cameroon, Rwanda, and Zambia using three separate methods. Here, inferences are based on 10 samples for both stairwayplot (grey line) and SMC++ (orange line), and 10 samples for MSMC (purple line).

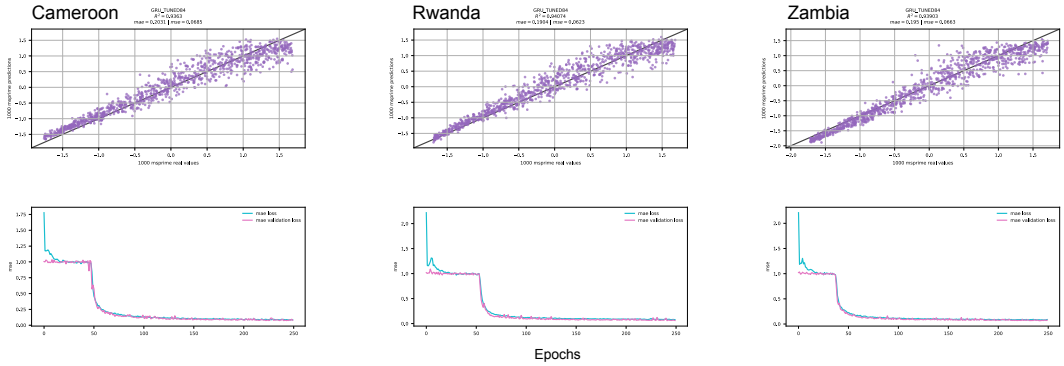


**Figure S23** ReLERNN test results for Cameroon, Rwanda, and Zambia when trained under assumptions of mutation-drift equilibrium. **(Top)** Scatter plot of raw (unnormalized) predictions for 1000 test examples using ReLERNN with the same parameters used in ***Figure 2***. Mean absolute error and mean squared error are shown for each population. **(Bottom)** Line graph showing the convergence of loss (measured by mean squared error) over time (epochs) during training on the same data as above, for both the training set (blue lines) and the validation set (purple lines).

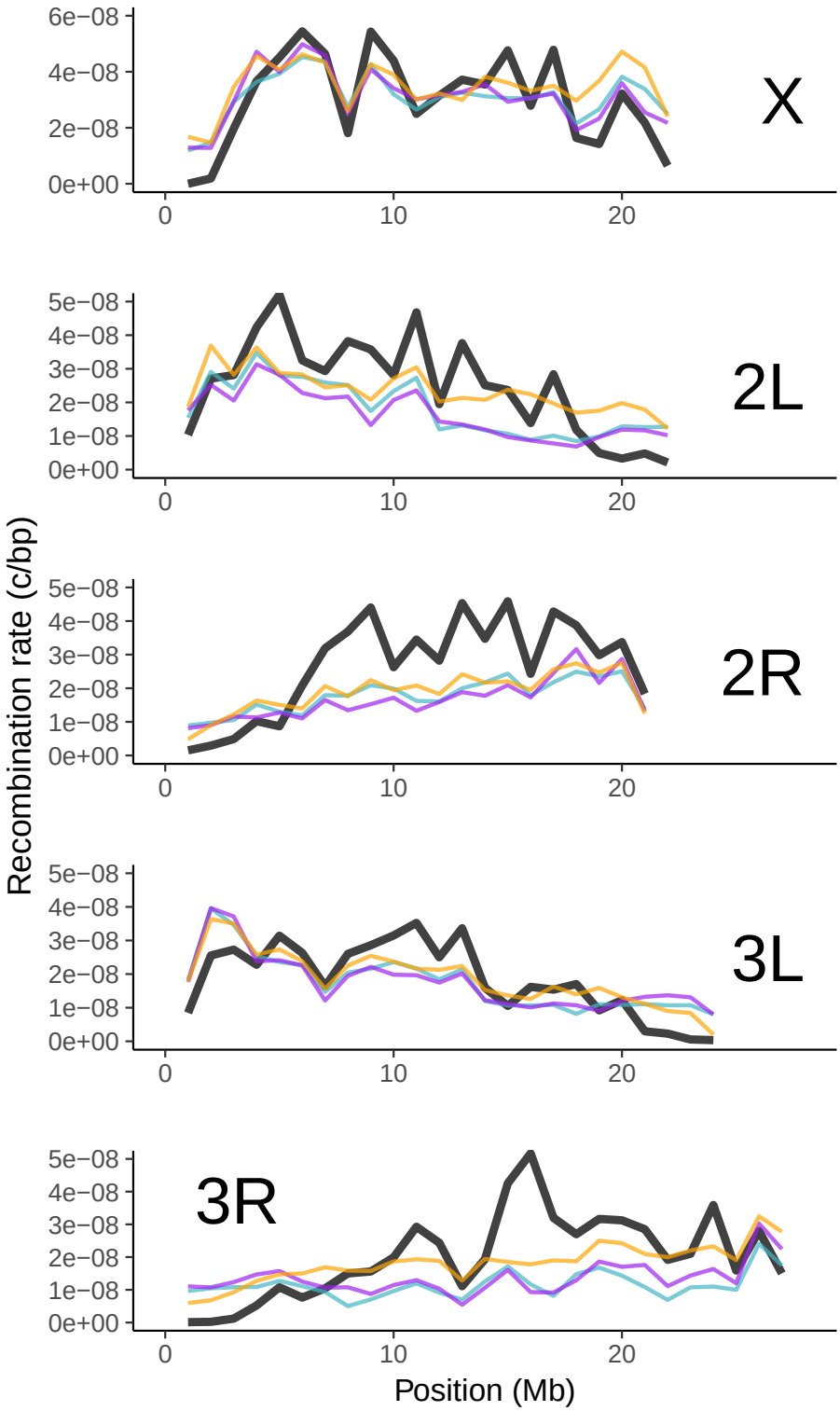


**Figure S24** Genome-wide recombination landscapes for *D. melanogaster* populations from Cameroon (teal lines), Rwanda (purple lines), and Zambia (orange lines). Rates are compared to those experimentally derived by ***Comeron et al.*** (***2012***) (black lines). All rates have been scales to 1 Mb windows by using a weighted average (see Materials and Methods). Sample sizes ($n = 10$) are the same for all populations.

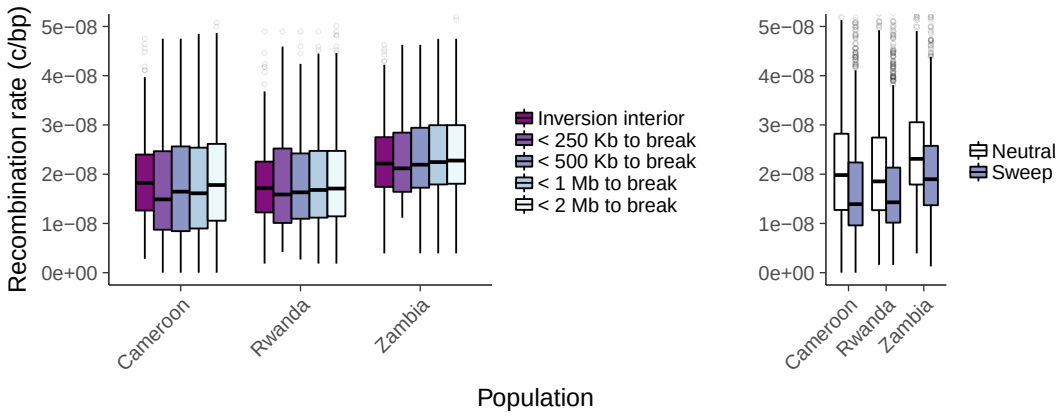


**Figure S25 (Left)** Recombination rate estimates for genomic windows > 2 Mb inside, < 250 kb surrounding, < 500 kb surrounding, < 1 Mb surrounding, and < 2 Mb surrounding all inversion breakpoints. **(Right)** Recombination rate estimates for all genomic windows overlapping windows predicted as either hard/soft sweeps (purple) or as neutral (white) by diploS/HIC (***Kern and Schrider, 2018***).

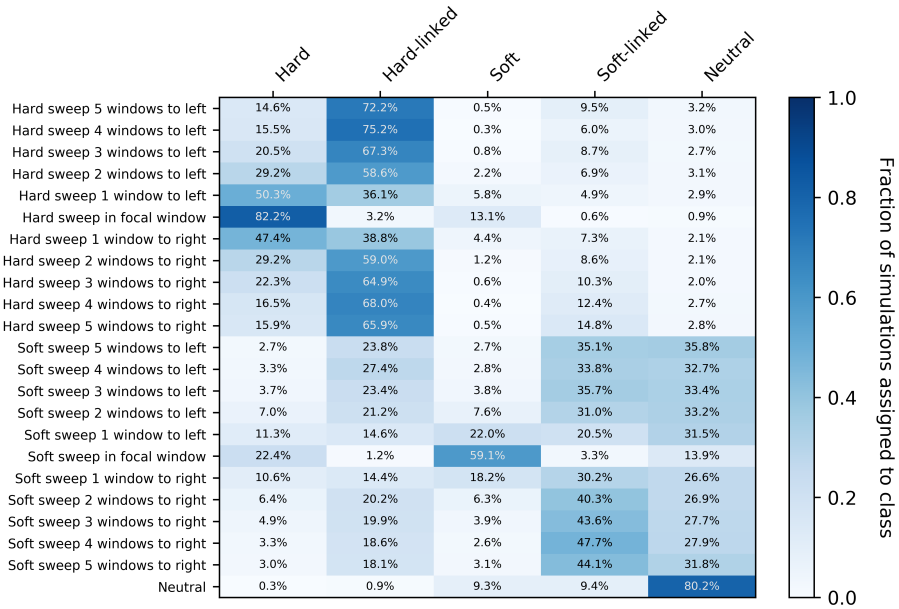


**Figure S26** Confusion matrix showing the fraction of test simulation windows assigned to each of five prediction categories by diploS/HIC (***Kern and Schrider, 2018***): hard, hard-linked, soft, soft-linked, and neutral. The y-axis shows the location of the window being classified relative to the selected window.

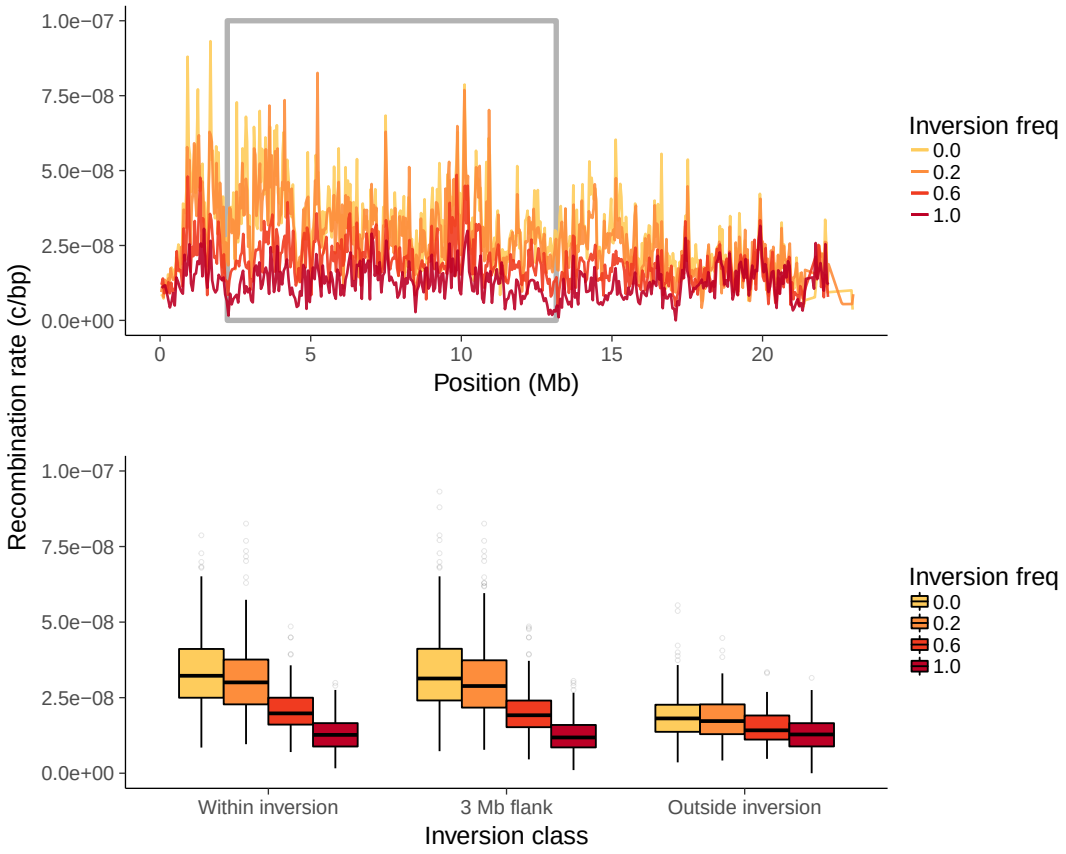


**Figure S27 (Top)** Recombination landscapes for Zambian *D. melanogaster* surrounding *In(2L)t*, sampled at different inversion frequencies. The grey box denotes the inversion boundaries of *In(2L)t* in *Drosophila* (***Corbett-Detig and Hartl, 2012***). **(Bottom)** Recombination rate estimates from genomic windows within the inversion, within a 3 Mb region flanking the inversion, and 3 Mb outside the inversion, sampled at different inversion frequencies.

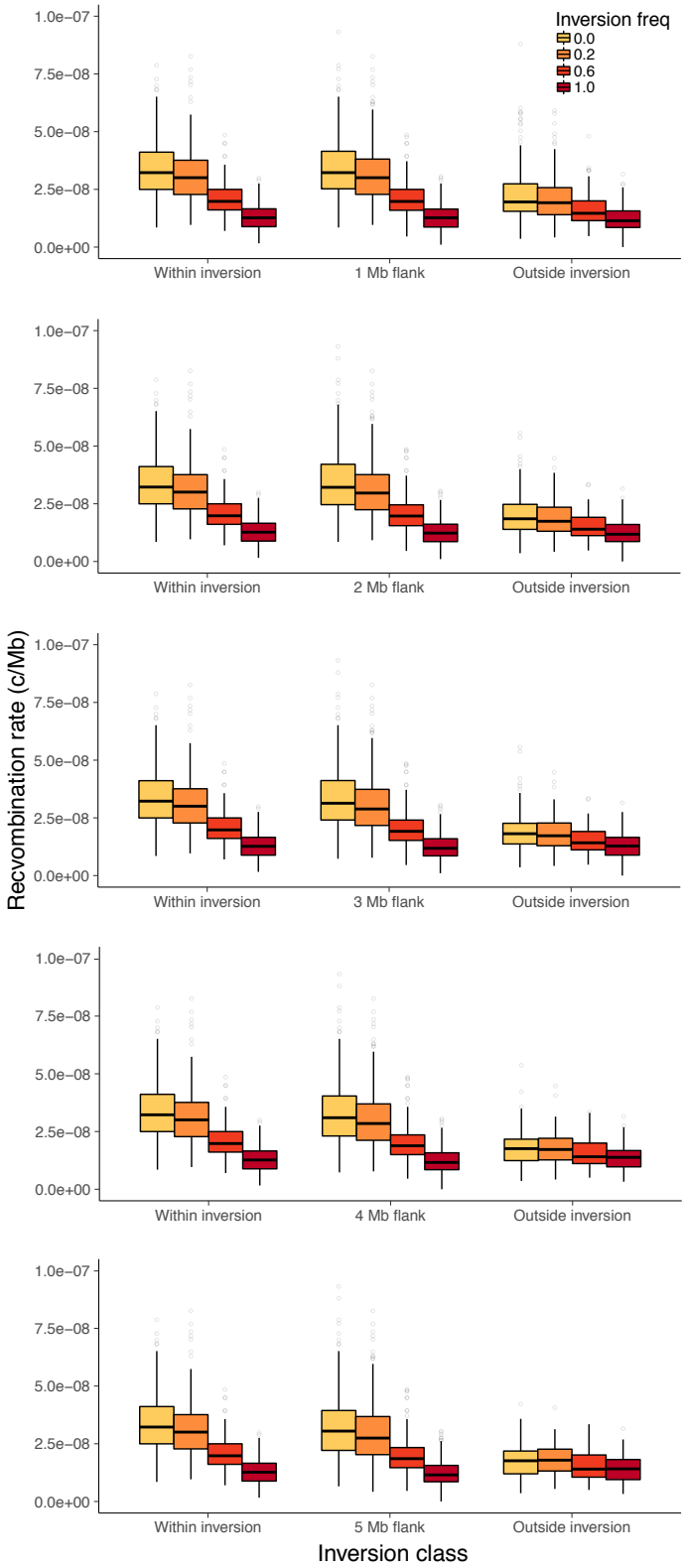


**Figure S28** Recombination rate estimates using flanking window sizes from 1-5 Mb. Rates are shown for genomic windows within the inversion, within regions flanking the inversion, and for regions outside both the inversion and flanking regions. All estimates are from chromosome 2L with *In(2L)t* sampled at different inversion frequencies